

Nanomechanical Spectroscopy of Ultrathin Silicon Nitride Membranes

S. S. Jugade, A. Aggarwal, A. K. Naik*

Centre for Nano Science and Engineering (CeNSE), Indian Institute of Science (IISc)

Bengaluru 560012, India

*E-mail: anaik@iisc.ac.in

Abstract

The mechanical properties of a nanomechanical resonator have a significant impact on the performance of a resonant Nano-electromechanical system (NEMS) device. Here we study the mechanical properties of suspended membranes fabricated out of low-pressure chemical vapour deposited silicon nitride thin films. Doubly-clamped membranes of silicon nitride with thickness less than 50 nm and length varying from 5 μm to 60 μm were fabricated. The elastic modulus and stress of the suspended membranes were measured using Atomic Force Microscope (AFM) based nanomechanical spectroscopy. The elastic modulus of the suspended membranes was found to be significantly higher than that of corresponding thin films on the substrate. A reduction in the net stress after the fabrication of membrane was observed and is explained by estimating the contributions of thermal stress and intrinsic stress. We establish a mathematical model to calculate the normalized elastic modulus of a membrane. Furthermore, we observe that the stress in a membrane changes with its length. We also develop an experimental model for the SiN_x membrane-Si substrate capillary force-gradient that could collapse the membrane.

Keywords – silicon nitride, membranes, atomic force microscopy, elastic modulus, stress, capillary condensation, pull-in

Silicon nitride nanomechanical resonators have potential applications as Nanoelectromechanical systems (NEMS) sensors¹⁻⁴ due to their high-quality factor (in the order of few millions) and high sensitivity at room temperatures.⁵⁻⁸ The fundamental natural frequency of a doubly clamped membrane resonator depends on its elastic modulus and stress as given below.⁹

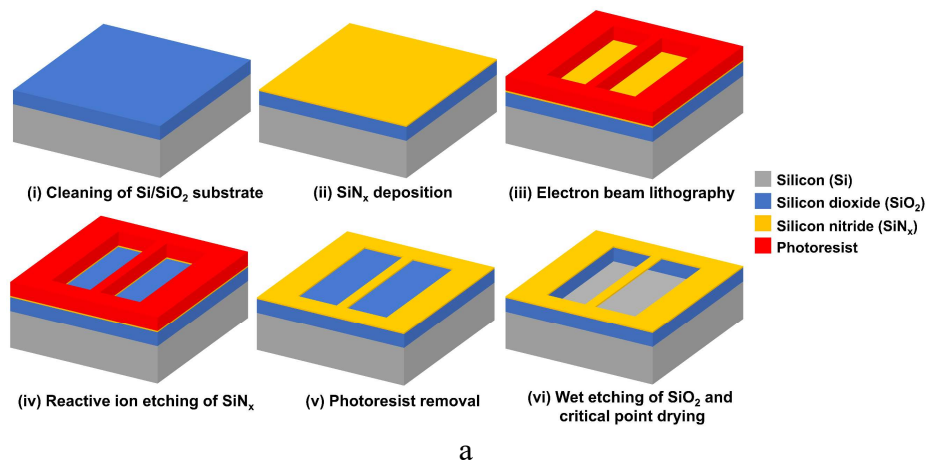
$$f_0 = 1.03 \sqrt{\frac{Et^2}{\rho L^4} + \frac{\sigma Wt}{3.4mL}} \quad (1)$$

where E is the elastic modulus, σ is the stress in the membrane, ρ is the density of the material, m is the effective mass, L, w and t are the length, width and thickness of the membrane respectively. Verbridge *et al.*¹⁰ have showed that the addition of tensile stress to the silicon nitride NEMS resonators leads to higher quality factors, that helps achieve higher sensitivity. Also, if the elastic modulus and stress of the membrane are very low, it is likely to collapse or undergo plastic deformation under a few nanonewtons of force. It is known that the mechanical properties of thin films, depending on the growth conditions, can vary significantly from that of the bulk material.¹¹⁻¹³ The Low-Pressure Chemical Vapor Deposition (LPCVD) grown silicon nitride films studied in this work have a thickness less than 100 nm and are amorphous in nature.¹⁴ Residual stress in thin films depend on the growth conditions: pressure, temperature, gas flow ratio, *etc.* The stress in an amorphous thin film can be separated into its intrinsic and thermal stress components.¹⁵ Intrinsic stress results from defects like voids, porosities, impurities, atomic diffusion, *etc.* And thermal stress is due to thermal expansion coefficient mismatch between film and substrate material.¹⁶ High tensile stress in the deposited films leads to cracks in the film and subsequent failure of the fabricated membrane. Hence, it becomes important to measure the elastic modulus of silicon nitride thin films and the suspended membranes fabricated out of them.

In this paper first, we describe the fabrication of suspended silicon nitride membranes. Then we explain the measurement techniques used to calculate the elastic modulus and stress of the suspended SiN_x membranes and corresponding thin films. Next, we compare the stress in the membranes and corresponding thin films. The variation of elastic modulus with the thickness of the membrane is analyzed using a model based on surface-energy considerations. The variation in stress with the length of the membrane is also studied. In the end, the capillary force-gradient between the membrane and bottom substrate is modeled based on the collapse of membranes.

Results and Discussion

LPCVD process was used to deposit silicon nitride films of thickness 47 nm, 51 nm and 88 nm on Si/SiO_2 substrate. The fabrication process of doubly-clamped membranes is illustrated in figure 1a. Figure 1b and 1c show a Scanning Electron Microscope (SEM) and Atomic Force Microscope (AFM) micrographs of a membrane respectively. The membrane is 5 μm in length and 500 nm in width. To prevent the collapse of membranes due to the charging effect, the SEM imaging of the actual membranes of 1-3 μm width to be used for the measurements was avoided.



a

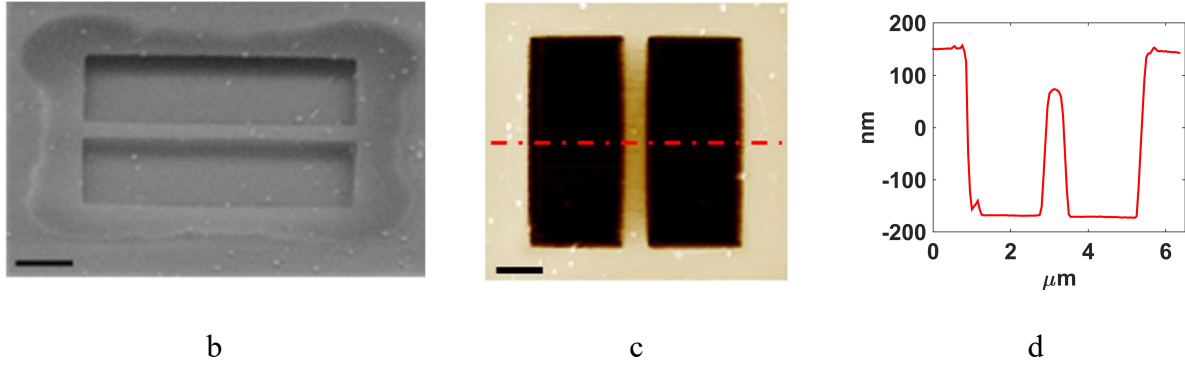


Figure 1. (a) The process flow for fabrication of a doubly-clamped silicon nitride membrane. (b), (c) SEM and AFM micrographs of a 5 μm long and 500 nm wide membrane respectively. (d) Topography of the section shown in figure 1c. Scale bar is 1 μm for figure 1b and 1c.

The elastic modulus and stress in the membrane were measured using AFM based indentation method.^{9,17,18} Central indentation experiments were performed with AFM using the force-distance (F-d) spectroscopy.^{19–21} The central indentation method is illustrated in figure 2a. Figure 2c is an AFM topography micrograph of a 5 μm long, 1.3 μm wide membrane fabricated from a 51 nm thick silicon nitride film. A Force vs. Deformation curve (figure 2d) was obtained after central indentation on the membrane. This curve was fitted using a force-deformation relation for a doubly clamped membrane subjected to central loading²² as given in equation (2). The coefficients of δ and δ^3 terms in equation (2) include elastic modulus and stress. Thus, the elastic modulus and stress values were obtained after fitting the Force vs. Deformation curve.

$$F = \left(16.23EW \left(\frac{t}{L} \right)^3 + 4.93\sigma \frac{Wt}{L} \right) \delta + 12.17E \frac{Wt}{L^3} \delta^3 \quad (2)$$

where E is the elastic modulus of the membrane, σ is the stress in the membrane, δ is the deformation in the membrane, L, W and t are length, width and thickness of the membrane.

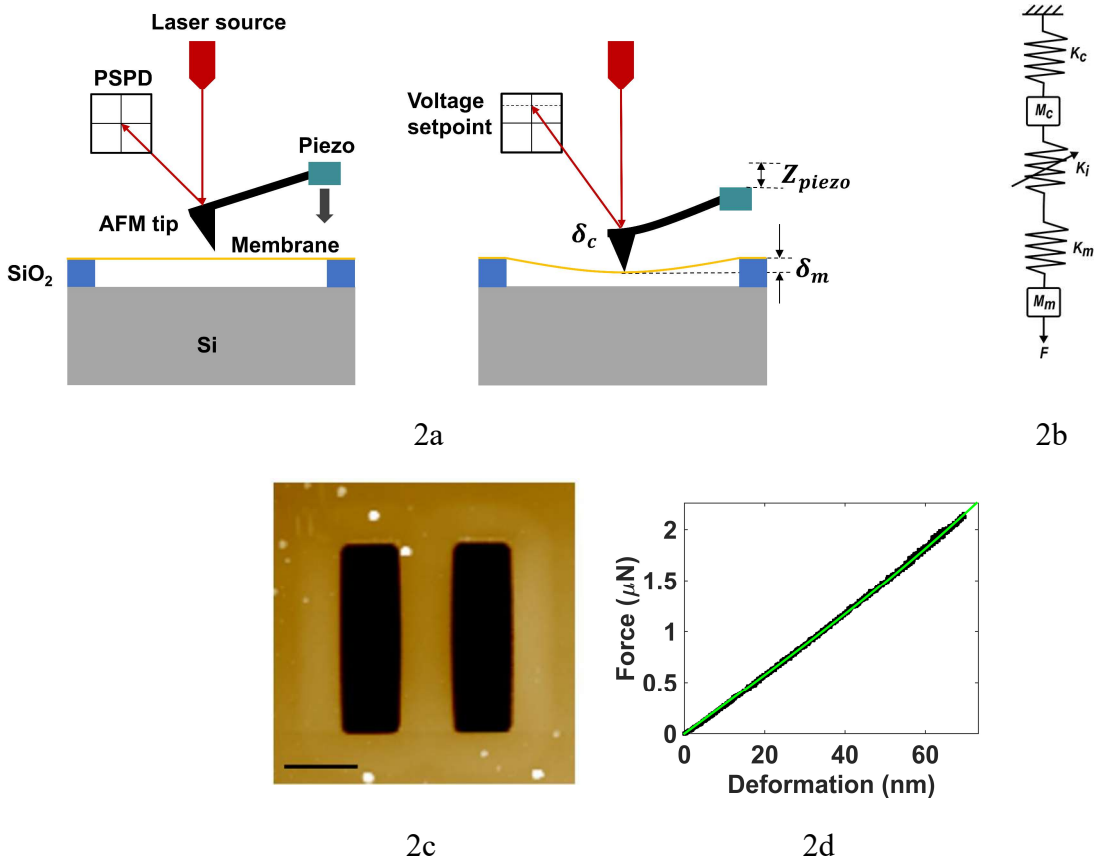


Figure 2. **(a)** Schematic of the AFM based central indentation method. **(b)** Equivalent spring-mass model of the system - K_c , K_i , and K_m are the stiffness of the AFM cantilever, tip-sample interaction, and membrane respectively. K_i is a variable stiffness. F is the applied force, M_c and M_m are the effective mass of the cantilever and the membrane respectively. **(c)** AFM topography micrograph of 5 μm long and 1.3 μm wide membrane fabricated from a 51 nm thick silicon nitride film. Scale bar is 2 μm . **(d)** Fitted Force vs. Deformation curve obtained on the same membrane after central indentation experiment.

The elastic modulus of the silicon nitride thin films on the substrate was measured using the nanoindentation ²³ technique. To find the stress in the films, the change in curvature of Si/SiO₂ substrate due to deposition of SiN_x film was measured using the beam deflection technique.¹⁶ Stoney's equation was then used to calculate the stress in the SiN_x film.²⁴ Due to a high deposition

temperature of 750°C, thermal stress is developed in the film when it was cooled down to room temperature. The contribution of thermal stress ¹⁶ to the net stress can be calculated as given below.

$$\sigma_{th} = \frac{E_f(\alpha_s - \alpha_f)\Delta T}{(1 - \vartheta_f)} \quad (3)$$

where σ_{th} is the thermal stress in the film. E_f , α_f and ϑ_f are the elastic modulus, coefficient of thermal expansion and poisson's ratio of the SiN_x film material. α_s is the coefficient of thermal expansion of the substrate material. ΔT is the difference between the deposition temperature and room temperature. For calculations, average values of $\alpha_f = 3.2 \times 10^{-6}/^\circ\text{C}$ (for SiN_x) and $\alpha_s = 0.65 \times 10^{-6}/^\circ\text{C}$ (for SiO₂) were considered.^{25,26} It is clear from equation (3), that the thermal stress will be larger in a film with higher elastic modulus than in a film with lower elastic modulus. Intrinsic stress in a film was calculated by subtracting the thermal stress from the net stress.

The elastic modulus, net stress, thermal stress, and intrinsic stress of the films are given in Table 1a. The elastic modulus of films of thickness 47 nm and 51 nm was very low i.e. about 10 % of the bulk modulus value of 270 GPa.²⁷ While the elastic modulus of 88 nm thick film was about 70% of the bulk value. The stress in each of the film was close to 1.5 GPa. The LPCVD process-parameters were the same for all the three films except for the 51 nm thick film, the gas flow ratio (NH₃: H₂Cl₂Si) was 10:100 unlike the ratio of 10:70 for the other two films. Increasing the gas flow ratio from 1:2 to 1:20 for nitrogen-rich LPCVD SiN_x films has a negligible effect on the residual stress.^{28,29} This explains why the stress in all the three films was almost equal. The contribution of thermal stress to the overall stress was negligible for the films of thickness 47 nm and 51 nm due to their low elastic modulus. While for the 88 nm thick film, thermal stress was about 30% of the total stress. The thickness of suspended membrane (Table 1b) was significantly lower than the thickness of corresponding film (Table 1a). This was because the SiN_x is also etched

during the wet etching of sacrificial SiO_2 with BOE. This reduction in the thickness can be expressed in terms of change in surface to volume ratio after the fabrication of membrane, $\Delta \left(\frac{S}{V} \right)$, given by equation (4). The reduction in the surface to volume ratio after the fabrication of membrane is 0.83, 0.42, and 0.49 for films of thickness 47 nm, 51 nm and 88 nm respectively.

$$\Delta \left(\frac{S}{V} \right) = \frac{t_f - t_m}{t_f} \quad (4)$$

Table 1a. Elastic modulus and stress of the SiN_x thin films measured using nanoindentation and beam deflection technique respectively

Thickness of deposited SiN_x film t_f (nm)	Elastic Modulus E_f (GPa)	Net stress σ_f (GPa)	Thermal stress σ_{th} (GPa)	Intrinsic stress σ_i (GPa)
47	20.54 ± 1.985	1.432 ± 0.114	0.054	1.378
51	28.52 ± 0.528	1.530 ± 0.190	0.075	1.455
88	184.5 ± 13.27	1.627 ± 0.259	0.487	1.140

Table 1b. Elastic modulus and stress of the 5 μm long and 1-3 μm wide suspended SiN_x membranes measured using AFM

Thickness of deposited SiN_x film t_f (nm)	Thickness of SiN_x suspended membrane t_m (nm)	Elastic Modulus E_m (GPa)	Stress σ_m (MPa)
47	8	104.1 ± 1.2	241.7 ± 1.5
51	30	222.6 ± 9.1	861.8 ± 2.7
88	45	204.1 ± 16.9	552.7 ± 4.5

It can be observed from Table 1a and 1b that stress in the membranes was significantly lower than that in the corresponding films. This reduction in stress after the fabrication of the membrane was due to the relaxation of thermal stress and intrinsic stress. The thermal stress relaxed because the suspended membrane was no longer attached to the substrate. The relaxation of thermal stress was negligible in membranes of thickness 8 nm and 30 nm, while 487 MPa of thermal stress was relaxed in case of 45 nm thick membrane. The relaxation of intrinsic stress depends on $\Delta \left(\frac{S}{V} \right)$ for the particular membrane. The reduction in the surface to volume ratio for the membrane of thickness 8 nm was 0.81, highest amongst all the three membranes. This means that most of the highly stressed regions of the 47 nm thick SiN_x film near the substrate were etched after fabrication of the membrane. Hence, there was a drastic reduction in stress from 1.432 GPa (for 47 nm thick film) to 242 MPa (for 8 nm thick membrane). The thermal stress in the 88 nm thick film was about six times higher than that in the 51 nm thick film (Table 1a). Hence, the net reduction of stress in the 45 nm thick membrane is higher than that in the 30 nm thick membrane (Table 1b). In fact, a few calculations reveal that relaxation of intrinsic stress in case of the membranes of thickness 30 nm and 45 nm was 593 MPa and 587 MPa respectively. So, the relaxation of intrinsic stress was about equal, that is also reflected through the very close values of 0.42 and 0.49 for $\Delta \left(\frac{S}{V} \right)$ of these two membranes.

The variation of elastic modulus, stress, and spring constant with the thickness of the membrane for a 5 μm length membrane are shown in figure 3a, 3b, and 3c respectively. The elastic modulus of the membranes was significantly higher than that of the corresponding films. The 30 nm thick membrane had a highest elastic modulus of 222 GPa (figure 3a). We expect the obtained elastic modulus values of membranes to be 15% higher than the actual values. Two main causes for this are the surface effects and offset of the tip from the center of the membrane during the indentation.

In AFM based indentation methods, repulsive interaction forces between the tip and surface of the membrane lead to a value of calculated elastic modulus higher than that of the actual.³⁰ Thermal drift in piezo and inclined motion of tip creates an offset of few tens of nanometers from the center of the membrane. The motion of tip is not in a direction perpendicular to the surface of membrane due to the repulsive forces between the tip and the membrane. These effects also lead to a higher value of calculated elastic modulus. Hence, for all further calculations, the elastic modulus of the membranes was taken 15% lower than the obtained values. The coefficient of linear deformation term (δ) in equation (2) gives the spring constant of the membrane. As shown in figure 3c the 8 nm thick membrane was around 8 times softer than the 30 nm thick membrane. While the membranes of thickness 30 nm and 45 nm had relatively same values of spring constant.

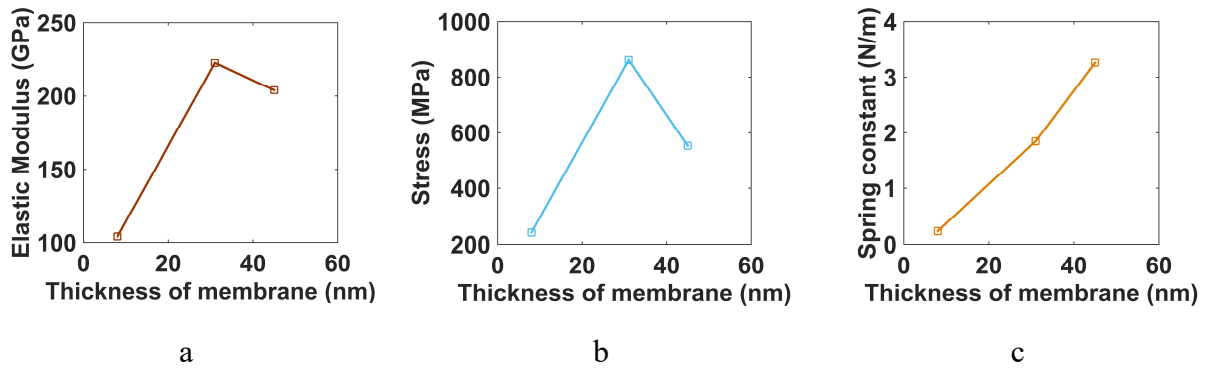


Figure 3. For a 5 μm length membrane, **(a)** Elastic modulus vs. Thickness of membrane. **(b)** Stress vs. Thickness of membrane. **(c)** Spring constant vs. Thickness of membrane.

The observed trend in the elastic modulus of suspended membranes was further investigated using a similar approach followed by Fedorchenko *et al.*³¹ A suspended membrane has both the top and bottom surfaces free. So, for surface energy calculations it can be considered as a thin film with its both surfaces free. For such a film, the limiting thickness t_0 below that it cannot be considered as a bulk material³¹ is given in equation (5).

$$t_0 = \frac{(1-\vartheta_f)}{E_{bulk}\varepsilon_0^2} \quad (5)$$

where ϑ_f is the poisson's ratio of the film = 0.3 (assumed), E_{bulk} is the bulk elastic modulus of the film material, ε_0 is the film strain. Table 2 has the calculated values of t_0 and ε_0 for the three membranes. The strain in the three membranes was different. Hence, a normalized thickness of a membrane was defined as the ratio of thickness of the membrane and the limiting thickness. Similarly, the normalized elastic modulus of a membrane was also defined.

Table 2. Limiting thickness (t_0) and strain (ε_0) values for the suspended membranes

Thickness of the membrane t_m (nm)	Strain in the membrane ε_0 ($\times 10^{-3}$)	Limiting thickness t_0 (nm)	Normalized thickness of the membrane $N_t = \frac{t_m}{t_0}$	Normalized elastic modulus of the membrane $N_E = \frac{E_m}{E_{bulk}}$
8	2.7	347.47	0.023	0.328
30	4.6	124.97	0.240	0.700
45	3.2	255.43	0.176	0.642

The normalized thickness of membranes clearly explains the calculated elastic modulus data. The 30 nm thick membrane has the highest normalized thickness hence it has the highest elastic modulus among all the three membranes. The variation in the normalized elastic modulus of membrane vs. the normalized thickness of membrane was expressed using equation (6). Curve fitting yielded a value of 0.272 ± 0.064 for p . The fitted curve is shown in figure 4a. Now, for any value of strain and thickness of membrane, equation (6) can be used to find the elastic modulus of the membrane.

$$N_E = (N_t)^p \quad (6)$$

For the membranes of thickness 30 nm and 45 nm, it was found that the stress changes with the length of the membrane. If the stress in a membrane does not change with its length then equation (7) is valid. But we found that there is a slight deviation from this behavior for membranes of thickness 30 nm and 45 nm (figure 4b and 4c). These values of $n < 1$ correspond to an increase in stress with the length of the membrane. This could be due to an increase in tensile stress redistribution with the increasing area of the membranes during the fabrication process. For 30 nm thick membranes, there was a gradual increase in stress from 652 MPa to 1011 MPa with the increase in length of membrane from 10 μm to 60 μm . But for membranes of thickness 45 nm, the increase in stress with the length of membrane is relatively small as the exponent n has a value close to 1 (figure 4c).

$$\frac{\sigma_m}{L} = C \frac{1}{L^n} \quad (7)$$

where, σ_m is the stress in the membrane, L is the length of the membrane, C is a constant and $n=1$.

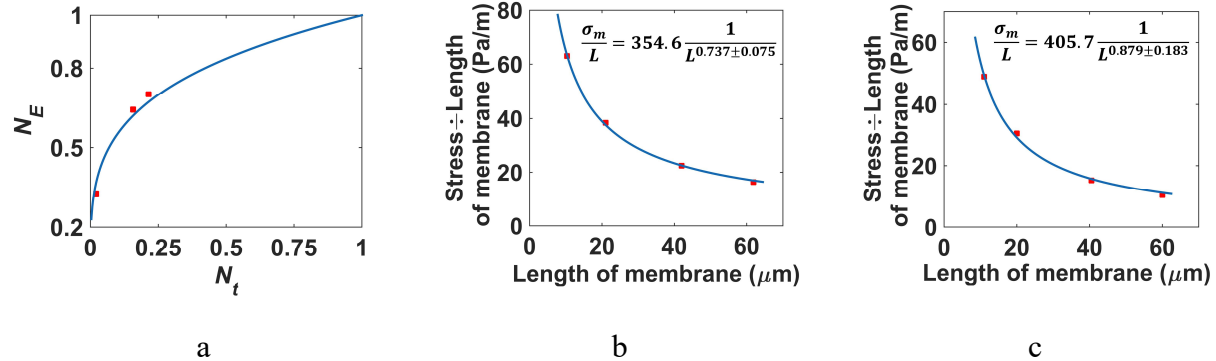


Figure 4. (a) Normalized elastic modulus vs. Normalized thickness of the membrane. (b), (c) Ratio of stress and length of membrane vs. Length of the membrane for membranes of thickness 30 nm and 45 nm respectively.

The membranes of thickness 30 nm collapsed to the bottom substrate under higher applied loads at the center of the membranes (figures 5a, 5b and 5c). Due to condensation of a water droplet, a liquid bridge (capillary) is formed between the surface of a membrane and the bottom substrate when they are very close to each other.^{32,33} This capillary adhesion force between the two surfaces collapses the suspended membrane. The pull-in of the membranes is illustrated in figure 6. The experimental parameters of the pull-in measurements are listed in Table 3. The point of the collapse of membrane is indicated by a sudden drop in force in the corresponding force-separation curve. Such an abrupt drop in force was due to the relaxation of the cantilever as the membrane moves down. During the pull-in of the membrane, the Z position of piezo did not change as the pull-in process took less than 1 milliseconds time.

The net relaxation of the cantilever in the region R (figure 5d, 5e, and 5f) is equal to the gap between the membrane and substrate at the start of the pull-in process. For the membranes of length 20 μm and 40 μm , the cantilever did not relax completely after the pull-in of the membrane was over (figure 5d, 5e, and 6a). While for the 60 μm long membrane, the cantilever relaxed completely before the pull-in was over and then lost contact with the membrane (figure 5f). As a result of the small gap, capillary condensation occurred between the cantilever and the membrane that is now attached to the substrate. This lead to snap-in of the cantilever to the membrane surface (figure 6b). In case of all the three membranes, the piezo moves down in Z direction and the tip presses down on the hard SiN_x on the Si substrate after the pull-in of the membrane is over. During this process, only the cantilever is deflected and that is why an infinite slope is observed in the force-separation curves. The cantilever continues to deflect until the force setpoint is reached. After this, the piezo retracts and cantilever pulls-off from the SiN_x surface by overcoming the capillary adhesion force (minimum of retract curve in figure 4a, 4b, and 4c). Also, the pull-in

process time (t_c) is three orders of magnitude greater than the inverse of the fundamental resonance frequency of the membranes ($1/f_0$). Hence, the dynamics of pull-in of the membranes is governed by viscous damping.

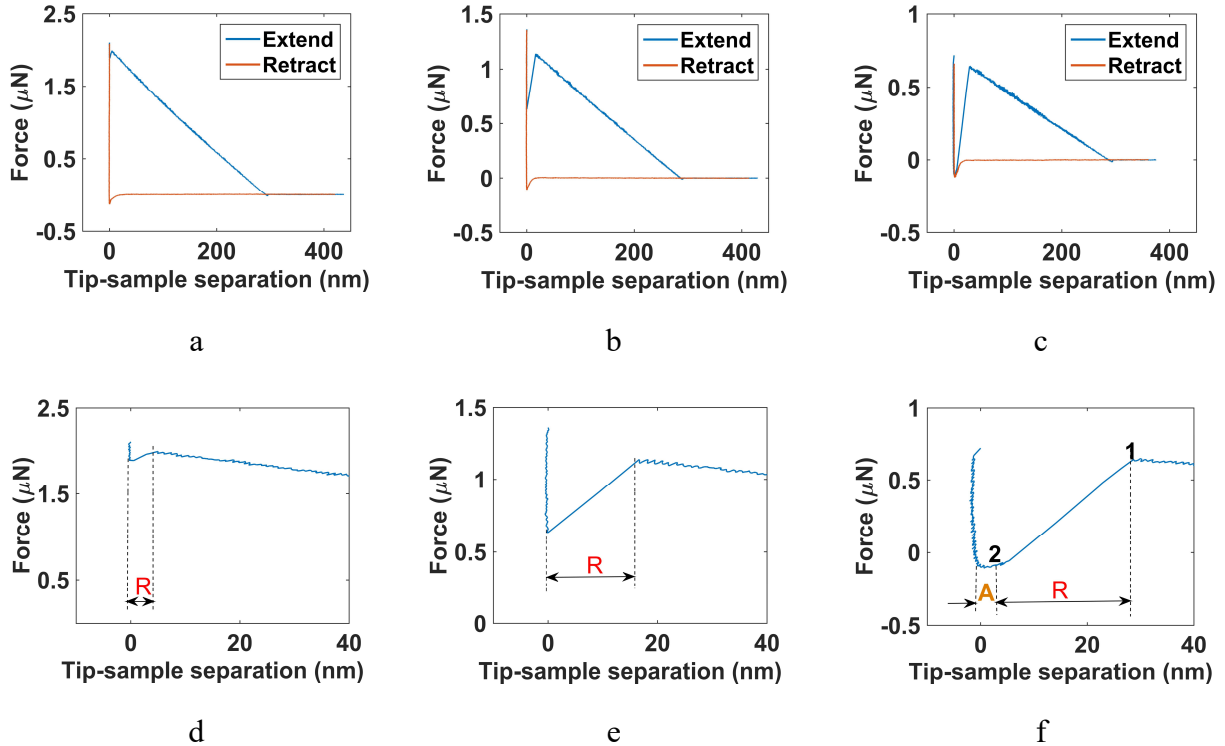


Figure 5. Force vs. Tip-sample separation curves indicating the collapse of 51 nm thick membrane. **(a)** For 20 μm long membrane. **(b)** For 40 μm long membrane. **(c)** For 60 μm long membrane. **(e), (f), (g)** Zoomed region of the Force vs. Tip-sample separation extend curve corresponding to the pull-in of membranes of length 20 μm , 40 μm and 60 μm respectively. The region R corresponds to the pull-in of the membrane. The slope of the curve in the region R is equal to the spring constant of the cantilever. The region A corresponds to the snap-in of the cantilever to the membrane.

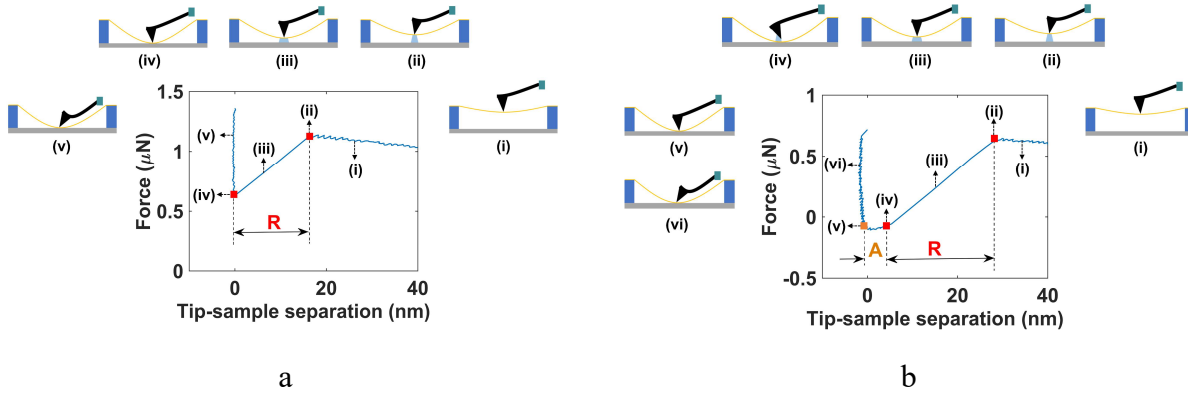


Figure 6. **(a)** Pull-in process illustrated for membranes of length 20 μm and 40 μm based on the force-separation curve for 40 μm long membrane. **(b)** Pull-in process illustrated for 60 long membrane based on its force-separation curve.

Table 3. Experimental parameters during pull-in measurements

Parameters	20 μm long membrane	40 μm long membrane	60 μm long membrane
Force on the cantilever at the start of the pull-in process, F_{cs} (nN)	1994	1140	643.9
Gap between the membrane and substrate at the start of the pull-in process, h (nm)	5.014	16.72	23.438
Force on the cantilever at the end of the pull-in process, F_{ce} (nN)	1888	628.6	-101.9
Capillary force gradient, $\frac{\partial F}{\partial h}$ (N/m)	-5.255	-0.4559	-0.2296
Pull-in process time, t_c (μs)	237	475	950
(Fundamental resonance frequency) $^{-1}$, $1/f_0$ (μs)	0.0526	0.0982	0.138

A membrane collapses when the sum of the capillary force gradient and stiffness of the membrane becomes zero as given in equation (8). The stiffness of the membrane was calculated as the negative of the slope of Force vs. Tip-sample separation extend curve in the region just before the collapse of the membrane. The obtained Capillary force gradient vs. Gap data was fitted using a power relation (equation 9) as shown in figure 7.

$$\frac{\partial F}{\partial h} + K_m = 0 \quad (8)$$

$$\frac{\partial F}{\partial h} = -138.6 h^{-2.03 \pm 0.001} \quad (9)$$

where, $\frac{\partial F}{\partial h}$ is the capillary adhesion force-gradient, K_m is the stiffness of the membrane and h is the gap between the SiN_x membrane and the bottom Si substrate.

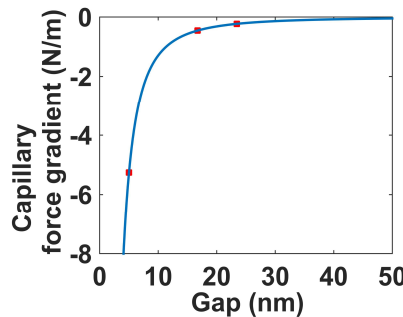


Figure 7. Capillary force gradient vs. Gap between the membrane and the bottom substrate

Integration of equation (9) shows that the capillary force varies as $\frac{1}{h^{1.03}}$ with the distance between the membrane and surface. This agrees well with the parabolic model for the capillary force between two parallel plates, wherein the force varies as $\frac{1}{h}$ with the distance between the plates.^{34,35} Thus, the capillary adhesion force gradient can be modeled as given in equation (9). Based on the above-mentioned model and experimental force-gradient, the contact angle was

calculated as 89.93° . This implies that the surfaces of SiN_x membrane and bottom Si substrate are hydrophobic in nature.

Conclusions

In summary, we have fabricated suspended silicon nitride membranes of thickness 8 nm, 30 nm, and 45 nm from the LPCVD high-stress SiN_x films of thickness 47 nm, 51 nm, and 88 nm respectively. Using AFM based indentation method, we studied the variation in elastic modulus and stress of a $5\ \mu\text{m}$ length membrane for three different thickness. Thermal stress in the films was relaxed after membrane-fabrication but the relaxation of intrinsic stress depends on the surface to volume ratio reduction after membrane-fabrication. Higher the surface to volume ratio reduction, higher will be the relaxation of intrinsic stress after the fabrication of the membrane. The values of elastic modulus obtained were about 15% higher than the actual ones due to surface effects and offset between the tip and center of the membrane. A model was developed to find the variation of normalized elastic modulus with the normalized thickness of the membrane. We found that the stress also depends on the length of the membrane, especially for the 30 nm thick membranes. This understanding of the variation of elastic modulus and stress in the membranes is important for developing more efficient NEMS resonators. Finally, based on the force-separation curves for the collapse of 30 nm thick membranes, we developed a mathematical model for the gradient of capillary adhesion force between the surface of SiN_x membrane and bottom Si substrate. The model predicts that the capillary force-gradient varies inversely with the square of the gap between membrane and substrate. This result can be particularly helpful in the design and fabrication of suspended membrane-based NEMS devices so as to prevent the failure due to condensation induced capillary adhesive forces.

Methods

Fabrication of suspended SiN_x membranes

The steps involved in the fabrication process were: (i) RCA cleaning of the Si/SiO₂ substrate. (ii) Deposition of LPCVD grown high-stress silicon nitride thin film on the substrate. The process parameters are listed in Table S1 of supplementary information. (iii) Spin-coating of PMMA A4 photoresist, followed by patterning of membrane-features for different dimensions using Electron beam lithography and then the development of photoresist using MIBK: IPA (1:3) developer. (iv) Reactive-ion-etching of silicon nitride from the windows opened in the lithography step using SF₆ gas. (v) Removal of PMMA using oxygen plasma. (vi) Wet etching of sacrificial silicon dioxide using 13:2 buffered oxide etch (BOE/BHF), followed by Critical Point Drying (CPD) to release the membranes.

AFM characterization of suspended SiN_x membranes

The topography of the membranes was acquired in AFM by scanning with a constant force of 10-40 nN in Peak Force Quantitative Nanomechanical Mapping (PFQNM)³⁶ mode in Bruker Dimension Icon AFM. The length and width of the membrane are determined from the topography micrograph. To measure the membrane thickness, a large force of about 10 μ N is applied to the membrane during the AFM scan. This force was sufficient for the suspended membrane to collapse to the bottom substrate. The step height is then measured in the region where the membrane is in contact with the bottom Si substrate.

Measurement of thickness of SiN_x thin films

The thickness of SiN_x films and SiO₂ layer was measured using Variable Angle Spectroscopic Ellipsometer (VASE)³⁷ J.A. Woollam Co. M2000U. The measurement is performed at an incident angle of 65°, 70°, and 75°. The thickness of the SiO₂ layer is 300 nm.

Measurement of elastic modulus and stress of SiN_x thin films

The elastic modulus of the silicon nitride thin films was measured using nanoindentation technique. Hysitron TI 950 Triboindenter with a Hysitron spherical diamond tip (radius 1 μ m) is used to indent the sample in load control mode. Loading and unloading Force vs. Displacement curves are acquired in a load control of 100 μ N, 180 μ N and 500 μ N for the films of thickness 47 nm, 51 nm, and 88 nm respectively. The elastic modulus is obtained by the fitting the unloading curve using the Oliver-Pharr model.^{38,39} To measure the stress of SiN_x films, the beam deflection technique was employed in a laser-based kSA Multi-beam Optical Sensor (MOS) system. The change in the curvature of the substrate is converted to stress in the film using Stoney's equation.

Acknowledgments

We acknowledge funding support from DST SERB through grant number EMR/2016/006479 and from LAM Research through 2018 Unlock ideas campaign. We also acknowledge funding support from MHRD, MeitY and DST Nano Mission through NNetRA. We thank Prosenjit Sen for helpful technical discussions.

References

1. Naik, A. K., Hanay, M. S., Hiebert, W. K., Feng, X. L. & Roukes, M. L. Towards single-molecule nanomechanical mass spectrometry. *Nat. Nanotechnol.* (2009).

2. Hanay, M. S. *et al.* Single-protein nanomechanical mass spectrometry in real time. *Nat. Nanotechnol.* (2012).
3. Chaste, J. *et al.* A nanomechanical mass sensor with yoctogram resolution. *Nat. Nanotechnol.* (2012).
4. Hiebert, W. Mass sensing: Devices reach single-proton limit. *Nat. Nanotechnol.* (2012).
5. Verbridge, S. S., Craighead, H. G. & Parpia, J. M. A megahertz nanomechanical resonator with room temperature quality factor over a million. *Appl. Phys. Lett.* **92**, 4–6 (2008).
6. Verbridge, S. S., Shapiro, D. F., Craighead, H. G. & Parpia, J. M. Macroscopic tuning of nanomechanics: Substrate bending for Reversible control of frequency and quality factor of nanostring resonators. *Nano Lett.* (2007).
7. Larsen, T. *et al.* Ultrasensitive string-based temperature sensors. *Appl. Phys. Lett.* (2011).
8. Schmid, S., Kurek, M., Adolphsen, J. Q. & Boisen, A. Real-time single airborne nanoparticle detection with nanomechanical resonant filter-fiber. *Sci. Rep.* (2013).
9. Frank, I. W., Tanenbaum, D. M., van der Zande, A. M. & McEuen, P. L. Mechanical properties of suspended graphene sheets. *J. Vac. Sci. Technol. B Microelectron. Nanom. Struct.* **25**, 2558 (2007).
10. Verbridge, S. S., Parpia, J. M., Reichenbach, R. B., Bellan, L. M. & Craighead, H. G. High quality factor resonance at room temperature with nanostrings under high tensile stress. *J. Appl. Phys.* **99**, (2006).
11. Alexopoulos, P. S. & O’Sullivan, T. C. Mechanical Properties of Thin Films. *Annu. Rev.*

Mater. Sci. **20**, 391–420 (1990).

12. Šimůrka, L., Erkan, S. & Turutoglu, T. Characterization of Silicon Nitride Thin Films on Glass. *Defect Diffus. Forum* **368**, 86–90 (2016).
13. Huang, H. *et al.* Effect of deposition conditions on mechanical properties of low-temperature PECVD silicon nitride films. *Mater. Sci. Eng. A* **435–436**, 453–459 (2006).
14. Joshi, B. C. *et al.* LPCVD and PECVD silicon nitride for microelectronics technology. *Indian J. Eng. Mater. Sci.* **7**, 303–309 (2000).
15. Vlassak, J. Thin Film Mechanics. *Harvard Univ.* (2004).
16. Evans, A. G. & Hutchinson, J. W. The thermomechanical integrity of thin films and multilayers. *Acta Metall. Mater.* **43**, 2507–2530 (1995).
17. Castellanos-Gomez, A., Singh, V., Van Der Zant, H. S. J. & Steele, G. A. Mechanics of freely-suspended ultrathin layered materials. *Ann. Phys.* **527**, 27–44 (2015).
18. Lee, C., Wei, X., Kysar, J. W. & Hone, J. Measurement of the elastic properties and intrinsic strength of monolayer graphene. *Science (80-.)*. (2008).
19. Cappella, B. & Dietler, G. Force-distance curves by atomic force microscopy. *Surf. Sci. Rep.* (1999).
20. Butt, H. J., Cappella, B. & Kappl, M. Force measurements with the atomic force microscope: Technique, interpretation and applications. *Surf. Sci. Rep.* (2005).
21. Seo, Y. & Jhe, W. Atomic force microscopy and spectroscopy. *Reports Prog. Phys.* (2008).

22. Senturia, S. *Microsystem Design*. (Kluwer Academic, 2000).
23. Wu, P. H. *et al.* Mechanical property characterization of sputtered and plasma enhanced chemical deposition (PECVD) silicon nitride films after rapid thermal annealing. *Sensors and Actuators, A Phys.* (2011).
24. Janssen, G. C. A. M., Abdalla, M. M., van Keulen, F., Pujada, B. R. & van Venrooy, B. Celebrating the 100th anniversary of the Stoney equation for film stress: Developments from polycrystalline steel strips to single crystal silicon wafers. *Thin Solid Films* (2009).
25. AZO Materials. Properties: Silicon Nitride (Si₃N₄) Properties and Applications. *AZO Materials* (2001). Available at: <http://www.azom.com/properties.aspx?ArticleID=53>.
26. AZoM. Silica-Silicon Dioxide. *AZO Materials* (2001). Available at: <https://www.azom.com/properties.aspx?ArticleID=1114>.
27. Askeland, D. R., Haddleton, F., Green, P. & Robertson, H. *The Science and Engineering of Materials*. (Springer US, 1996).
28. Gardeniers, J. G. E., Tilmans, H. A. C. & Visser, C. C. G. LPCVD silicon-rich silicon nitride films for applications in micromechanics, studied with statistical experimental design*. *J. Vac. Sci. Technol. A Vacuum, Surfaces, Film.* **14**, 2879–2892 (1996).
29. Noskov, A. G., Gorokhov, E. B., Sokolova, G. A., Trukhanov, E. M. & Stenin, S. I. Correlation between stress and structure in chemically vapour deposited silicon nitride films. *Thin Solid Films* **162**, 129–143 (1988).
30. Ni, H. & Li, X. Young's modulus of ZnO nanobelts measured using atomic force microscopy and nanoindentation techniques. *Nanotechnology* **17**, 3591–3597 (2006).

31. Fedorchenko, A. I., Wang, A. B. & Cheng, H. H. Thickness dependence of nanofilm elastic modulus. *Appl. Phys. Lett.* **94**, (2009).
32. Cheng, S. & Robbins, M. O. Capillary adhesion at the nanometer scale. *Phys. Rev. E - Stat. Nonlinear, Soft Matter Phys.* (2014).
33. Cheng, S. & Robbins, M. O. Nanocapillary Adhesion between Parallel Plates. *Langmuir* (2016).
34. *Surface Tension in Microsystems*. (Springer, 2013).
35. Valsamis, J.-B. A study of liquid bridges dynamics: an application to micro-assembly. (Université libre de Bruxelles).
36. Minne, S. C., Hu, Y., Hu, S., Pittenger, B. & Su, C. NanoScale Quantitative Mechanical Property Mapping Using Peak Force Tapping Atomic Force Microscopy. *Microsc. Microanal.* (2010).
37. Woollam, J. A. & Snyder, P. G. Fundamentals and applications of variable angle spectroscopic ellipsometry. *Mater. Sci. Eng. B* (1990).
38. Taylor, J. A. The mechanical properties and microstructure of plasma enhanced chemical vapor deposited silicon nitride thin films. *J. Vac. Sci. Technol. A Vacuum, Surfaces, Film.* **9**, 2464–2468 (1991).
39. Pharr, G. M. & Oliver, W. C. Measurement of Thin Film Mechanical Properties Using Nanoindentation. *MRS Bull.* (1992).

Supplementary Information

1. Low-Pressure Chemical Vapour Deposition (LPCVD) process parameters

The silicon nitride thin films were deposited on a Si/SiO₂ substrate by Low-Pressure Chemical Vapour Deposition (LPCVD) process. The important process-parameters are listed below.

Table S1. LPCVD process-parameters

Thickness of SiN _x film (nm)	Gas-flow ratio (Dichlorosilane: ammonia) (sccm:sccm)	Deposition pressure (mTorr)	Deposition temperature (°C)
47	10:70	300	750
51	10:100	300	750
88	10:70	300	750

2. Central indentation method

Figure S1 illustrates the measurement setup for the central indentation experiment. Initially, the AFM tip is located above the center of the membrane at a distance where there was no interaction between the tip and membrane atoms. Then the piezo moves down in Z direction resulting into deformation of the membrane and deflection of the cantilever. The piezo extends down until a voltage setpoint is reached on the position sensitive photodiode (PSPD). Then it retracts to its original position. Thus, Voltage vs. Z-piezo curve was obtained for extending and retract motion at a rate of 1 Hz. The velocity of piezo during extension and retraction motion is 1 $\mu\text{m/sec}$.

The Voltage vs. Z-piezo curves is obtained after central indentation on the membrane shown in the AFM micrograph (figure S2a). Based on the deflection sensitivity and spring constant

calibration values¹ these curves were converted to Force vs Z-piezo curves as shown in figure S2b. The Force vs Z-piezo curves were then converted to Force vs Separation curves (figure S2c) using Eq. (SE1).² The applied force and corresponding deformation were obtained by calculating the separation value for the jump to contact point when the tip approaches the sample (figure S2d). Thus, a Force vs. Deformation curve was obtained as shown in figure S2e.

$$Z_{\text{piezo}} = \delta_m + \delta_c \quad (\text{SE1})$$

where, Z_{piezo} is the displacement of the piezo in the Z direction, δ_m is the deformation of the suspended membrane and δ_c is the deflection of the cantilever.

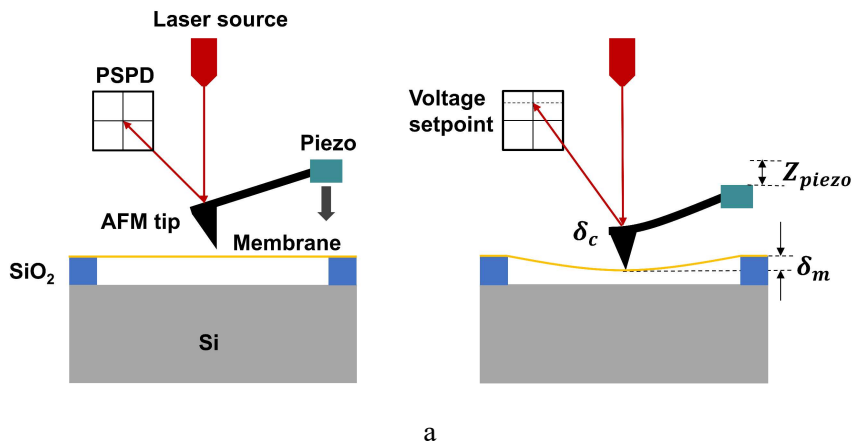


Figure S1. Schematic of the measurement setup for AFM based indentation method. Deformation of the membrane and deflection of the cantilever due to piezo motion in the Z direction.

The spring constant of the selected cantilever was such that there was significant deformation of the membrane with a detectable voltage difference on PSPD. The spring constant of the cantilever used for the membranes fabricated from 51 nm and 88 nm thick films was 31 N/m. For the relatively softer membranes fabricated from 47 nm thick film, a cantilever of spring constant 17 N/m was used. The spring constant was calibrated using the thermal tuning.³ The indentation depth on SiN_x films using the above cantilevers was less than 0.5 nm. Hence, there was no pressing

effect of the tip ⁴ during the indentation of the membranes. The tip radius was very small (< 40 nm) compared to the membrane length ($> 5 \mu\text{m}$) and width ($> 1 \mu\text{m}$). This ensured that the elastic modulus and stress values were not affected by the tip radius.

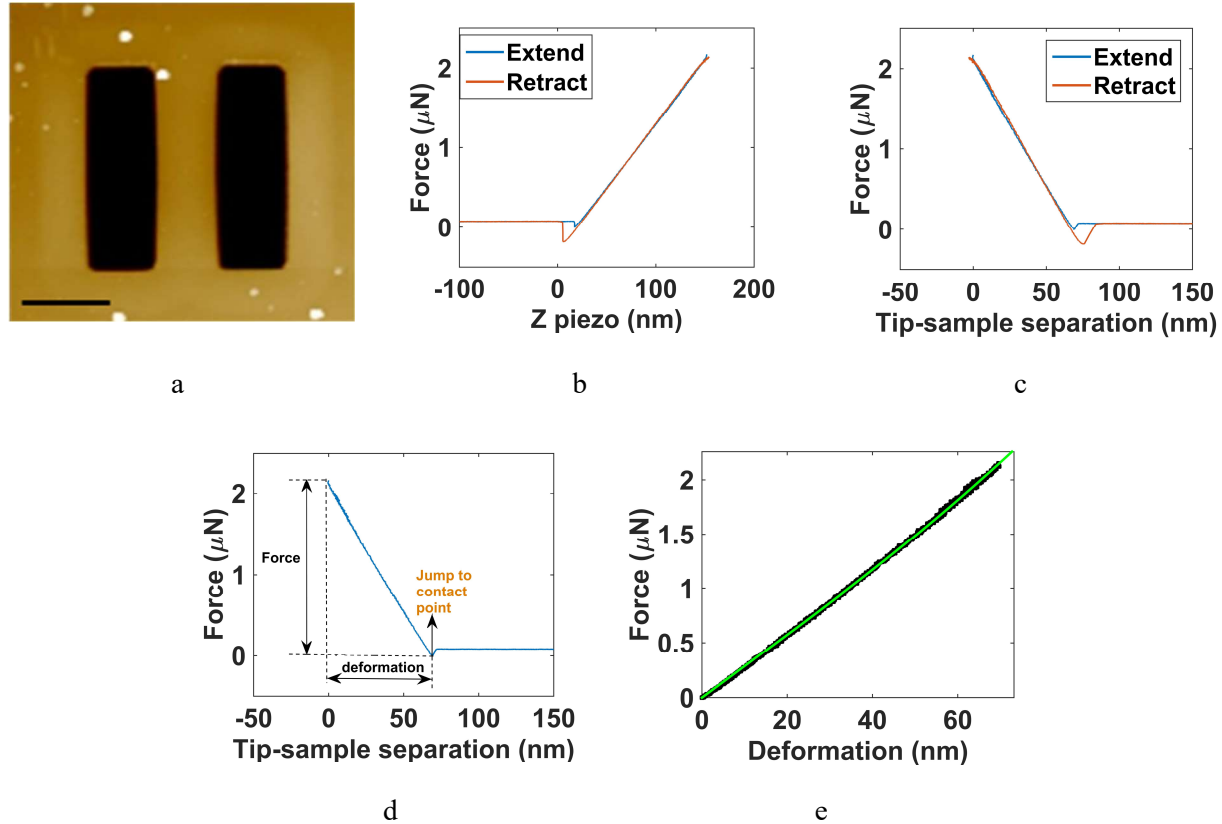


Figure S2. (a) AFM topography of $5 \mu\text{m}$ length, $1.3 \mu\text{m}$ width membrane fabricated from a 51 nm thick silicon nitride film. Scale bar is $2 \mu\text{m}$. (b), (c), (d) Force vs. Z piezo, Force vs. Tip-sample Separation curves and Extend Force vs. Tip-sample separation curve obtained on the same membrane after central indentation experiment respectively. (e) Force vs. Deformation curve for the membrane in figure S2a.

3. Model for capillary force-gradient

The model for the capillary force between two parallel plates based on a parabolic meniscus ⁵ (figure S3a) is given below.

$$F(h) = -\pi\gamma R^2 \left(\frac{-2Cot\theta}{h} + \frac{4}{4R-hCot\theta} \right) + 2\pi\gamma R Sin\theta \quad (SE2)$$

where γ is the surface tension of water, R is the wetting radius, $Cot\theta$ is the cotangent of the average of the contact angles on the top and bottom surface, h is the gap between the two plates. For $4R \gg hCot\theta$, Eq. (SE2) becomes Eq. (SE3). Differentiating Eq. (SE3), we obtain the force-gradient as a function of the gap between the two plates.

$$F(h) = -\pi\gamma R^2 \left(\frac{-2Cot}{h} + \frac{1}{R} \right) + 2\pi\gamma R Sin\theta \quad (SE3)$$

$$\frac{\partial F}{\partial h} = -\pi\gamma R^2 \left(\frac{2Cot\theta}{h^2} \right) \quad (SE4)$$

The SiN_x suspended membrane and bottom Si substrate can be modeled as two parallel plates along a cross-section passing through the center of the membrane and parallel to its width. The capillary force gradient found by fitting the experimental data is given in Eq. (SE5). The modeled force-gradient varies as $\frac{1}{h^2}$ with the gap. While the experimental force-gradient varies as $\frac{1}{h^{2.03}}$ with the gap. Hence, by comparing Eq. (SE4) and (SE5), the coefficient of h^{-2} in R.H.S of Eq. (SE4) was obtained. The wetting radius was assumed to be half of the width of the membrane ($\approx 500 \text{ nm}$). This is a valid assumption as all the points on the membrane-surface along its width will be at a same height from the bottom substrate. The variation of the wetting radius with the contact angle is shown in figure S3b. Based on this assumption, the contact angle was calculated as 89.93° .

$$\frac{\partial F}{\partial h} = -138.6 h^{-2.03 \pm 0.001} \quad (SE5)$$

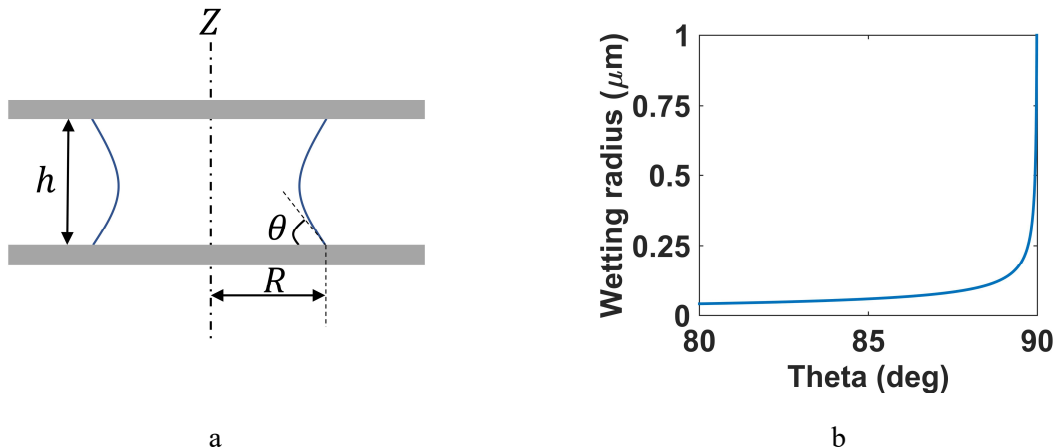


Figure S3. (a) Parabolic meniscus between two parallel plates. (b) Variation of the wetting radius with the contact angle.

References

1. Butt, H. J., Cappella, B. & Kappl, M. Force measurements with the atomic force microscope: Technique, interpretation and applications. *Surf. Sci. Rep.* (2005).
2. Frank, I. W., Tanenbaum, D. M., van der Zande, A. M. & McEuen, P. L. Mechanical properties of suspended graphene sheets. *J. Vac. Sci. Technol. B Microelectron. Nanom. Struct.* **25**, 2558 (2007).
3. Burnham, N. A. *et al.* Comparison of calibration methods for atomic-force microscopy cantilevers. *Nanotechnology* (2003).
4. Ni, H. & Li, X. Young's modulus of ZnO nanobelts measured using atomic force microscopy and nanoindentation techniques. *Nanotechnology* **17**, 3591–3597 (2006).
5. Valsamis, J.-B. A study of liquid bridges dynamics: an application to micro-assembly. (Université libre de Bruxelles).